IEEE Access
Multidisciplinary ⋮ Rapid Review ⋮ Open Access Journal

Received 15 December 2023, accepted 24 December 2023, date of publication 1 January 2024,
date of current version 10 January 2024.

Digital Object Identifier 10.1109/ACCESS.2023.3349090

RESEARCH ARTICLE

Directional-Guided Motion Sensitive Descriptor for Automated Detection of Hypertension Using Ultrasound Images

ANJAN GUDIGAR[1], NAHRIZUL ADIB KADRI[2], U. RAGHAVENDRA[1], JYOTHI SAMANTH[3], MAHESH ANIL INAMDAR[4], MUKUND A. PRABHU[5], AND U. RAJENDRA ACHARYA[6]

[1]Department of Instrumentation and Control Engineering, Manipal Institute of Technology, Manipal Academy of Higher Education, Manipal, Karnataka 576104, India
[2]Department of Biomedical Engineering, Faculty of Engineering, University of Malaya, Kuala Lumpur 50603, Malaysia
[3]Department of Cardiovascular Technology, Manipal College of Health Professions, Manipal Academy of Higher Education, Manipal 576104, India
[4]Department of Mechatronics, Manipal Institute of Technology, Manipal Academy of Higher Education, Manipal 576104, India
[5]Department of Cardiology, Kasturba Medical College, Manipal Academy of Higher Education, Manipal 576104, India
[6]Centre for Health Research, School of Mathematics, Physics, and Computing, University of Southern Queensland, Springfield, QLD 4300, Australia

Corresponding author: U. Raghavendra (raghavendra.u@manipal.edu)

This research work was supported by the Science and Engineering Research Board (SERB) International Research Experience Fellowship for the year 2023–2024 funded by SERB, a statutory body of the Department of Science and Technology, Government of India, under Grant SIR/2022/000809.

ABSTRACT The current work proposes an efficient assessment of hypertension (HTN) using a Directional-Guided Motion Sensitive (DGMS) descriptor and Machine Learning (ML) algorithm. The main objective of the proposed work is to automate the detection of HTN using ultrasound (US) images. The four-chamber US images from 70 healthy subjects and 70 HTN patients are collected. A novel pipelined architecture has been developed in two stages with four phases: preprocessing, feature extraction using DGMS descriptor, feature ranking and selection, and classification using shallow K-Nearest Neighbor classifier. The proposed model has achieved a classification accuracy of 98% using a set of prominent features, predominating the performance attained by other approaches. This study suggests US contains predictive signals even when standard measures are normal and lays the groundwork for artificial intelligence-assisted cardiac assessment to aid quicker, more objective diagnosis and earlier treatment. If further validated on additional diverse patient data, the technology could be integrated into clinics to enhance HTN detection through automated, early discernment of subtle manifestations missed by human eyes and traditional metrics.

INDEX TERMS Computer aided diagnostic tool, directional-guided descriptor, hypertension, shallow classifier, ultrasound images.

I. INTRODUCTION

Hypertension (HTN) is one of the leading causes of cardiovascular disease (CVD) morbidity and mortality. HTN is diagnosed when a consistent systolic Blood Pressure (BP) reading is $\geq$ 140 mmHg and/or diastolic BP of $\geq$ 90 mmHg [1], [2], [3]. Based on office BP recordings, global prevalence of HTN is 32% in adults aged between 30 and 79 years [4]. Major cardiovascular complications of HTN include ischemic heart disease, myocardial infarction, sudden death, heart failure, ischemic stroke, hemorrhagic stroke, end-stage renal disease, and peripheral artery disease [5], [6]. The risk of complications is independently related to the presence of Hypertensive-Mediated Organ Damage (HMOD) among HTN patients [7]. HMOD refers to the presence of structural or functional changes in arteries or end organs (heart, brain, eyes, kidney, and blood vessels) caused by elevated BP. Several important HMODs such as cardiac, retinal, and vascular changes become markers of preclinical/asymptomatic CVD and have shown prognostic significance in HTN patients even in the absence of other cardiovascular risk factors [8]. The presence of single or

The associate editor coordinating the review of this manuscript and approving it for publication was Riccardo Carotenuto.

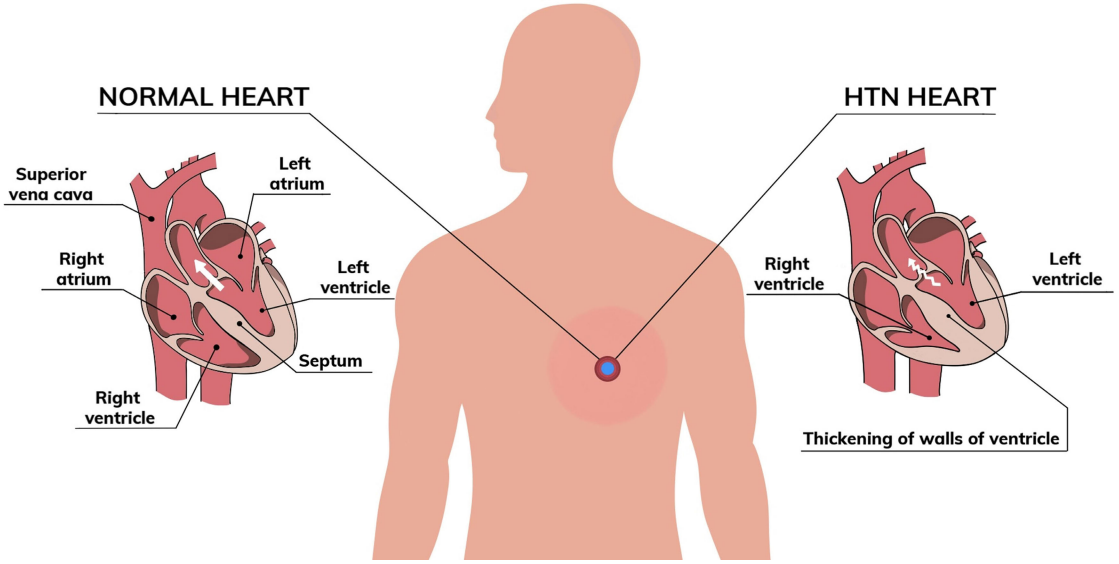

FIGURE 1. Structure of normal and HTN heart.

multiple forms of HMOD is common (not rare) and possesses a significant increase in cardiovascular risk [9], [10], [11]. Screening and detection of these HMODs are essential in the evaluation of patients with HTN for risk stratification and prognostication. Common patterns of HMOD are Left Ventricular Hypertrophy (LVH), arterial stiffening, and Chronic Kidney Disease (CKD) with albuminuria and proteinuria [12].

Based on the presence and extent of HMOD and other comorbidities, HTN can be classified as uncomplicated Stage 1 HTN, asymptomatic Stage 2 HTN, and established disease with Stage 3 HTN. Figure 1 shows the structural difference between normal and HTN hearts. These stages along with individual BP recording status have been used in the scoring for the risk stratification of cardiovascular disease [13]. In this aspect evaluation of patients with HTN requires thorough clinical history, physical examination, and diagnostic tests to rule out HMODs and other morbidities.

Throughout the disease, the heart is the important end organ that shows changes in HTN patients. The chronic burden of increased workload to the left ventricle (LV) leads to LVH, abnormalities in the LV relaxation, development of arrhythmias (atrial fibrillation), and heart failure. HTN increases the workload to the heart leading to structural and functional alteration in the heart. The spectrum of proven cardiac changes in HTN is also denoted as hypertensive heart disease that ranges from asymptomatic LVH to advanced heart failure. This includes diastolic heart failure with preserved LV ejection fraction, systolic LV failure, or a combination of both. Such patients with uncontrolled HTN are disposed to acute cardiac events such as decompensated heart failure, acute coronary syndrome, or sudden cardiac death. HTN also disrupts the endothelial function on the arterial wall layer, which becomes the precursor for the development of atherosclerotic plaque on the vessel wall. This provokes the development of coronary artery disease and peripheral artery disease. Evaluation of the heart is one of the key steps in the assessment and management of these HTN patients [14], [15], [16].

Electrocardiography (ECG) is the first line of diagnostic tests that can be used to evaluate for the presence of LVH and arrhythmias. The incidence of LVH in ECG is directly related to the severity of HTN. As the ECG exhibits poor sensitivity in the diagnosis of LVH, Echocardiography is recommended as this influences the treatment decision [14], [15], [16], [17]. 2D Trans Thoracic Echocardiographic (TTE) diagnosis of LVH is a strong predictor of mortality in HTN and general populations [18], [19]. 2D TTE assessment will also provide detailed information on LV geometry, chamber volume, and function [18], [20]. Echocardiography is also used to evaluate the aortic size and diagnose coarctation of the aorta, one of the causes of secondary HTN.

Further, screening for blood vessel-related HMOD, carotid ultrasound, pulse wave velocity, and ankle-brachial index is used. Carotid intima-media thickness and plaques can be quantified using carotid artery ultrasound imaging which predicts cardiovascular risk [21], [22]. Carotid-femoral pulse wave velocity is efficient in the diagnosis of arterial stiffness [23]. Screening for CKD is an important part of the evaluation process as HTN stands the second most common cause of CKD [24], [25]. Additionally, fundoscopy is used in the diagnosis of hypertensive retinopathy [26]. Meanwhile, HTN also increases the prevalence of brain damage in the form of transient ischemic attack and stroke. However subtle asymptomatic changes in the brain have been documented in Magnetic Resonance Imaging (MRI) scans in HTN patients [27], [28]. New onset HTN may show cardiac findings similar to that of normal well-being. Furthermore, HTN cannot be diagnosed based on one reading. In a few circumstances, office BP recording shows high readings, while the true BP remains normal which is termed white coat HTN. Meanwhile, few demonstrated masked HTN features

where office BP recording shows the normal range and home reading shows elevated BP About 10% to 30% of patients with high BP readings have white coat HTN and 10% to 15% of them will have masked HTN. Hence the diagnosis of HTN necessitates multiple BP readings checked during at least 2 to 3 office visits along with 1 to 4 weeks intervals unless the BP is more than 180/110mmHg [29]. Because of this variability, it would be prudent to have a modality that doesn't depend just on the BP measurement but incorporates other measurements to improve the accuracy of the diagnosis [29]. Echocardiographic evaluation holds good when it is associated with LVH. Whereas in the early stages, LVH may not be evident among them, and the LV size and structure may appear normal. In addition, manual interpretation of HTN and HMOD requires specialists and may lead to human errors. This raises the need for automated evaluation tools in patients who are diagnosed with HTN which may demonstrate an objective way to assess subtle myocardial changes in the heart. Hence, computer aided diagnostic (CAD) tools have been developed by various researchers as one of the prospective solutions using Ultrasound (US) images to avoid human errors [30], [31], [32], [33], [34]. US imaging of heart - echocardiography is the widely used imaging modality in the evaluation of heart diseases. Patients visiting the cardiology department invariably undergo echocardiographic testing for the evaluation of the heart's structure and function. In this aspect, US imaging of the heart in HTN patients facilitates the evaluation and extent of cardiac involvement in them. US imaging is a feasible diagnostic test and is lower priced than MRI and computed tomography. Hence, we used the US imaging modality for this research study.

II. LITERATURE REVIEW

Generally, CAD tools are widely used for the automated classification of medical images, signals, and clinical attributes. A survey was conducted from 2007 to 2016 on U.S. residents related to demographic, health, and nutrition information etc., and the National Health and Nutrition Examination Survey database was prepared (http:www. cdc.govnchsnhanes.htm). In [35], a study on this database using an artificial neural network-based model is conducted to evaluate the association of BMI, smoking, age etc., on hypertensive patients. The study attained an Area Under Curve (AUC) of 0.77 suggesting it can be used as a complementary tool to assist clinicians in recognizing high-risk hypertension patients. In [36], Mahalanobis (MAH) distance was used to detect HTN by removing multivariate outliers. The next stage was the predictive analysis for the detection of HTN. In this stage, the dataset was applied to multiple algorithms, and it was found that the MAH algorithm with random forest have attained an accuracy of 99.48%. Apart from questionnaire-based studies, research was also conducted to detect hypertension using various modalities such as ECG [37], [38], [39], US images [30], [31], and Photoplethysmography (PPG) signals [40], [41], A machine learning (ML)-based approach was proposed to detect patients with the probability of developing pulmonary hypertension (PH) [42]. The study utilized the data from an electronic health record (EHR) database. The model has a prediction rate of 0.92 Area Under the Curve - Receiver Operating Characteristic curve (AUROC). This model also categorizes the pulmonary arterial hypertension and chronic thromboembolic pulmonary hypertension subjects. The local interpretable model was used for the identification of hypertension using ECG signals [39]. They have used PhysioNet database and hospital database collected from Yanbian University Hospital, China. They have achieved an accuracy of 93.33% for the database collected from the hospital database. In [39], the hybrid approach is proposed by combining a Convolutional Neural Network (CNN) and Support Vector Machine (SVM) to categorize hypertensive and normotensive using ECG signals. However, Ballistocardiograph (BCG) showed a better result of 92.21% accuracy using K-Nearest Neighbor (KNN) classifier [43]. In [31], US images are categorized using a Globally Weighted Local Binary Pattern (GWLBP) with entropy and SVM classifier resulting in $\sim$ 92% accuracy. Various ML-based techniques are proposed by researchers for the detection of HTN. However, the training time needed for these models is a concern since most models take a sufficiently longer time [44]. The utilization of various feature selection techniques may help in optimizing the models thus making it readily available for clinicians in real-time scenarios.

We have reviewed and summarised related work for the detection of hypertension using various modalities. We know that it is just the exploration of available related work and not follow the systematic review process. However, the systematic review approach can be further explored for the benefit of stakeholders, researchers, and doctors in the future. Table 1 shows the findings of various approaches in terms of used modalities, methods, and results.

A. LITERATURE GAPS

From Table 1 it is observed that there are very few works reported for the automated detection of HTN based on ML and deep learning techniques using various modalities. However, the method using US images has achieved maximum specificity and sensitivity, as compared to the other methods. It is also noted that only two works are available using heart US images. Furthermore, the utilization of heart US images for the identification of HTN helps to understand the structural changes of cardiac in HTN patients. Therefore, we proposed to capture a micro-level texture descriptor for US four-chamber heart images. Though it is very significant research work, there is a dearth of publicly available four-chamber heart US images. The four-chamber view of the heart in US imaging depicts all 4 chambers of the heart, i.e. left atrium, left ventricle, right atrium, and right ventricle. Increased BP in HTN patients directly increases the workload on the left ventricle, which pumps the blood

TABLE 1. Various methods for the detection of hypertension using ML-based and deep learning approaches.

Sl. No	Ref	Method	Modality	Database	Results
1.	[37]	Hybrid deep model	ECG	139 recordings (PhysioNet) Test:156 samples	Avg. Acc.: 98% Avg. Sen. & Spe.:97%
2.	[38]	Entropy	ECG lead II + heart sound signal	Normal: 54 PH: 50 patients	Sen.: 74% Spe.: 87%
3.	[39]	CNN + SVM	ECG	PhysioNet: Normal:80 Hypertensive:139 (online) Private: Normal:40 Hypertensive:34	Acc.: 93.33%, Sen.:100%, Spe.:87.5%
4.	[40]	Deep learning approach	Arterial BP + PPG	ICU dataset MIMIC III:1732 subjects	MAE 1.31 systolic BP MAE 2.41 diastolic BP
5.	[43]	Integrated tunable Q-factor wavelet transform + KNN	BCG	figshare :128 BCG records	Acc.:92.21%, Sen.:92.96%, Spe.:91.60%
6.	[45]	Various ML-based algorithms	Echocardiographic data	Patients: 90	AUC: 0.87
7.	[30]	Various transform methods + graph embedding + decision tree	US images	Normal: 51 images HTN: 61 images	Acc.: 99.11% Sen. & Spe.:100%
8.	[31]	GWLBP + entropy+ SVM	US Images	Normal:49 subjects PH:49 patients	Acc.: 91.77%, Sen.:96%, Spe.:87.33%
9.	[42]	ML-based approach	EHR	Control: 11,279,478 PH: 115,822	AUROC:0.92 (PH)
10.	[46]	Deep learning approach	Chest radiographs + pulmonary artery systolic pressure	Healthy:357 PH:405 patients	AUC: 0.97
11.	[47]	ML-based classification	Lifestyle-related details	AGES	AUCROC: 0.978 and 0.990 (HTN/ diabetes)

*Acc.: accuracy, Sen.: sensitivity, Spe.: specificity, AUCROC: Area Under Curve Receiver Operating Curve, MAE: Mean Absolute Error

towards the aorta with high BP. Also, in advanced stages of HTN, the left atrium tends to dilate to compensate for the left ventricular filling pressure that is altered due to increased stress. As the four-chamber view displays the long axis view of the left ventricle and left atrium, we extracted these images for the development of an Artificial Intelligence (AI)-based automated detection model.

The literature gaps are identified and listed as given below.

- There is a lack of publicly available four-chamber US heart image datasets for research. This work provides a substantial dataset of 4200 images.
- Prior studies utilize only small image datasets (112 images total across existing works). This work leverages 4200 images to better represent disease variability.
- Most existing works rely on signals or clinical attributes rather than cardiac imaging data for HTN detection. This work is among the first to demonstrate ultrasound's capabilities.
- No prior study extracts micro-level texture features sensitive to structural manifestations in the heart. This work pioneers a directional guided motion descriptor for subtle texture characterization.

In summary, by using a sizable dataset and novel imaging-based analysis using granular texture features, this work addresses significant data and methodological gaps impeding progress. The high accuracy achieved underscores ultrasound's potential and the utility of an integrated CAD system for enhanced diagnostic support.

B. MOTIVATION AND OUR PROPOSED APPROACH

Clinical suspicion for HMOD increases based on the history and presentation. Cardiac changes in the form of LVH and LV diastolic impairment are the most prevalent changes that can be seen in HTN patients. Certainly, echocardiography is a feasible diagnostic method for cardiac structural and functional abnormalities, this has been widely used in the evaluation of HTN patients. Yet, cardiac structure and function may remain normal as per the echocardiographic evaluation, especially during the early stages of HTN, where echocardiography cannot rule out HTN. Subtle changes in

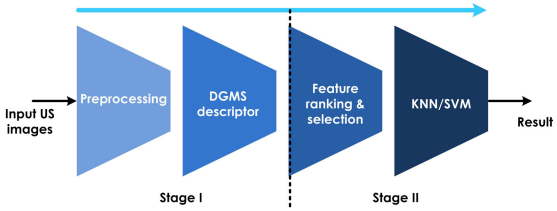

FIGURE 2. Architectural illustration of the proposed method.

the myocardium may not be picked by the human eye. On this facet, we aimed to compare cardiac US images of HTN patients and healthy controls drawn from transthoracic echocardiography to develop an automated identification model in the evaluation of HTN. In this regard, we have collected four chamber US heart images from more number of patients and tested the proposed model with the same.

The proposed method comprises two key stages i.e., Stage I and Stage II. In Stage I: Initially, the binary mask superimposing technique on the input US images is used to acquire only a four-chamber heart view. Further, a novel texture descriptor i.e., Directional-Guided Motion Sensitive (DGMS), based on pixel directions is used to extract the microlevel texture features from the preprocessed US heart images. These features help to extract the discriminative feature vectors among normal and HTN hearts. In Stage II: To reduce the dimensionality of the feature vector, we have incorporated feature ranking using an entropy-based technique and are selected based on its significance values. Further, the selected features are classified using shallow classifiers to predict HTN conditions in the heart. Moreover, the performance measures showed that the proposed DGMS descriptor on US heart images contributes to producing discriminative features. The rough idea of our approach is illustrated in Figure 2. A detailed description of the proposed method is given in the following sections.

C. CONTRIBUTIONS

The main contributions of the proposed work are listed below,

- The identification of HTN using four chamber heart images is a critical research area, liable to human bias. To contribute to this area of research, we have proposed a novel descriptor to capture the heart motion.
- To the best of our knowledge, first time we have spawned the new database which comprises a greater number of four-chamber healthy and HTN heart US images.
- The proposed system achieved a promising accuracy of 98% using a reasonably small set of significant handcrafted features with the help of a shallow classifier.

III. MATERIALS AND METHODS

A. DATASET DESCRIPTION

This retrospective study included cardiac US images drawn from 70 HTN patients (mean age 48 $\pm$ 8 years) and 70 healthy controls (mean age 46 $\pm$ 10 years). The study protocol was approved by the institutional ethics committee. Patients

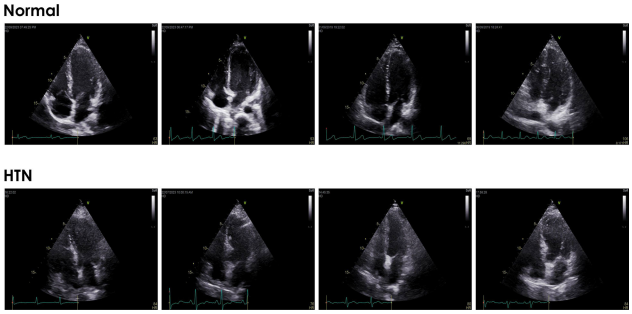

FIGURE 3. Some example images of normal and HTN used in the study.

with significant valvular problems, congenital heart disease, ischemic heart disease, patients not in sinus rhythm or having irregular heart rates, and cardiomyopathies were excluded from the study. Recorded apical four-chamber view loops for each participant was obtained from the Vivid S-60 echocardiographic machine, GE Healthcare system.

These four chamber view clips were recorded and gated with ECG including $\geq$1 cardiac cycle. Based on corresponding ECG waveforms we further extracted 15 images from the diastolic phase (frames between the second half of the T wave to Q wave) and 15 from the systolic phase (frames between R to first half of the T wave) from each participant's data. Hence there were 30 images drawn per individual subject. Overall, there were 2100 images in the HTN group and 2100 in the control group. Figure 3 shows the sample US images used in the present study.

B. APPROACH DESCRIPTION

In this section, we present a detailed pipelined description of Stages I and II of the proposed approach.

1) STAGE I

Stage I comprises two main blocks namely, preprocessing and DGMS descriptors. The detailed description is presented in the below section.

a: PREPROCESSING

This is the primary step in which the irrelevant information such as heart rate signal, grayscale margin, some labels, etc., are removed and the region of interest (ROI) i.e., four-chamber heart image is extracted. The irrelevant information is removed by cropping the image using empirically selected image coordinates. Further, we have generated the binary mask using the method available in [48] as shown in Figure 4. The generated mask is then superimposed on every input image to get the ROI. Subsequently, the median filter of size 5 $\times$ 5 is applied to improve the quality of ROI and eliminate the noise. Finally, the obtained images are resized to 256 $\times$ 256 to preserve the generality and it offers superior results when using handcrafted feature techniques [48], [49].

b: DGMS DESCRIPTOR

The micro-level texture features play a significant role in interpreting the underlying variations present in

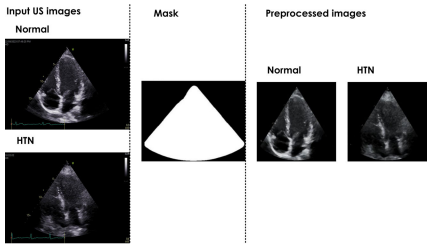

FIGURE 4. Preprocessed images generated using a binary mask.

four-chamber heart images. Hence DGMS descriptor is proposed to discriminate normal and HTN heart US images. Figure 5 shows the complete architectural flow for computing the DGMS feature vector and the detailed description is given below.

Consider a pixel coordinate (u_c, v_c) of an image I is I_C (i.e., central pixel) and $I_P(P = 0, 1, \ldots., 7)$ be the surrounding pixels of the I_C for an image patch 3×3 excluding the central pixel, as shown in Figure 5. As used in the Local Directional Pattern (LDP), we have incorporated 8 Kirsch masks (K_M) which are employed in directions of nearby pixels $I_P(P = 0, 1, \ldots., 7)$ [50]. Hence for these directions, it determines the variations in the intensity. Further the 8 Kirsch mask responses MR_P, w.r.t the pixel intensities $I_P(P = 0, 1, \ldots., 7)$ are computed. Individually these pixels are assigned to a digit between zero to seven based on its weight (i.e., with less intensity l_N) in the original image according to the magnitude of the Kirsch mask responses (i.e.,$|MR_P|$). Herein threshold δ is considered as 4, so that 50% of the selected surrounding pixels are assigned by 1 and others are 0, to balance pixel weightage.

Then the DGMS value is determined by

$$DGMS(u_c, v_c) = \sum_{N=0}^{7} g\left(I_N - I_C\right).2^{l_N} \tag{1}$$

where,

$$g(s) = \begin{cases} 1, & \text{if } s \geq 0. \\ 0, & \text{otherwise.} \end{cases} \tag{2}$$

and N is the pixel position in the new path as shown in Figure 5.

This new path helps to get the edge responses in a zig-zag way, which predominantly preserves the inherent motion of the heart valve. Once the DGMS coding is performed on the entire four-chamber heart image, the non-overlapping blocks with different sizes are generated on the resultant image (i.e., $b_o, o = 1, 2 \ldots, 6$). These non-overlapping blocks are empirically selected to extract the areas of the pixel of interest. Finally, the histograms are computed on non-overlapping blocks (i.e., hb_o) and are concatenated to form the DGMS feature model as described in (3), which is expected to represent the local micro-level structure of the heart.

$$\text{DGMS feature model} = hb_1 \| hb_2 \| hb_3 \| hb_4 \| hb_5 \| hb_6 \tag{3}$$

where, $\|$ is the concatenation operator.

2) STAGE II

Stage II comprises two main blocks namely, Feature ranking and selection, and classification. The detailed description is presented in the below section.

a: FEATURE RANKING AND SELECTION

The main rationale of the feature selection is to eliminate unnecessary information and keep the significant features. Thus, improves the performance of the ML algorithm by reducing the feature dimensions [51]. To be specific, our problem of concern is binary classification, wherein feature sets belong to normal and HTN. Hence, we have used an entropy-based ranking approach to calculate the p-value and criterion [52]. It uses the relative entropy (i.e., Kullback-Leibler distance) measures to evaluate the significance of the features [52]. Herein the features with maximum divergence are considered as more appropriate for separating the classes. Hence the ranking of features is performed by arranging them in descending sequence by the criterion value. Finally, a set of features are selected based on the $p < 0.001$. This process allowed us to obtain the best feature vector, which is further used to train and test various classification method.

b: CLASSIFICATION

In the pursuit of an effective classification solution, we embarked on the classification task after feature selection utilizing two primary techniques: KNN [53] and SVM [54]. To enhance the diversity and quality of our extracted features, we delved deeper into these techniques by employing a range of sub-techniques. The information on all these techniques has been mentioned below in brevity.

c: KNN

It is a simple and effective ML algorithm used for classification and regression tasks. It operates by assigning a data point's class label based on the majority class of its KNN in the training dataset. KNN's performance can be influenced by the choice of K hyperparameter, namely Fine KNN with K = 1 [55], [56], Medium with K=10 [55], [56] and Coarse with K=100 [55], [56] and in terms of distance metric used for neighbor identification. We employed Cosine KNN [55], [56] with cosine distance, Cubic KNN [55], [56] with a cubic distance metric and lastly, weighted KNN [55], [56] with weighted distance metric i.e., weighing nearby neighbors more heavily. These improve the classification task and help broaden the spectrum of feature representations.

d: SVM

It is a powerful supervised ML algorithm. It works by finding a hyperplane that maximizes the margin between different classes, effectively separating data points into distinct categories. SVM is particularly effective in high-dimensional spaces and can handle both linear and non-linear data separation using pertinent kernel functions; here we leveraged linear kernel for linearly separable data and a host of non-linear

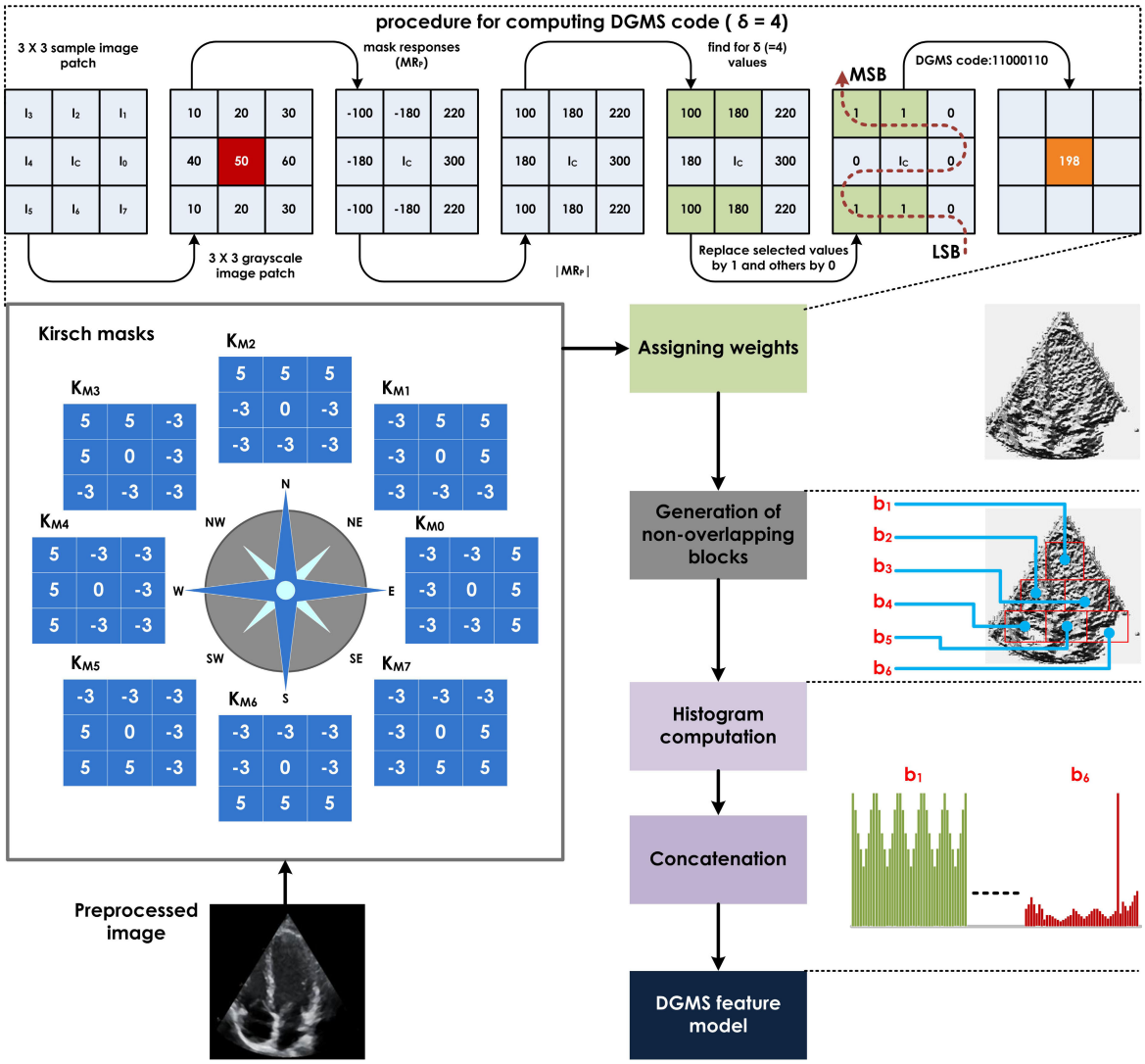

FIGURE 5. Illustration of generation of DGMS descriptor.

kernels for non-linear data, namely Gaussian (radial basis functions) [57], [58].

$$G(x_a, x_b) = exp\left(-\frac{|x_a - x_b|^2}{2\sigma^2}\right) = exp(-r\,|x_a - x_b|^2) \quad (4)$$

where, $r = \sqrt{\frac{q}{4}}$ for fine Gaussian, $r = \sqrt{q}$ for median Gaussian.

For polynomial functions [58], [59]

$$G(x_a, x_b) = \left(1 + x_a^T x_b\right) \quad (5)$$

where, σ represents the width of the kernel, q is the number of features or the dimension size of x_i and x_a, x_b are feature points.

We explore many variants within these to improve the robustness and accuracy of our classification results, namely fine [58] and median Gaussian [58] function median Cubic and quadratic polynomial functions [59] for the former and latter respectively. These facilitated the extraction of a wide array of feature representations, each tailored to the nuances of our dataset.

IV. EXPERIMENTAL RESULTS

In the current study, we have proposed a novel descriptor called DGMS descriptor or feature model. In this section, we have presented the results obtained using this descriptor. The complete proposed model is implemented on a system with the following specifications: Core i5-1235U, 1.30 GHz and RAM of 8 GB. We have used MATLAB R2022a environment to develop and test the proposed model. Initially, the feature of size 1536 is extracted using 256 × 256 preprocessed four-chamber heart images. The coding was performed for δ=4. Further, the significant features are selected using an entropy-based ranking method. We have selected highly ranked 585 features with p<0.001. The selected significant features are further classified using a 10-fold cross-validation approach. For the classification, the MATLAB classification learner tool is utilized. Herein shallow classification models

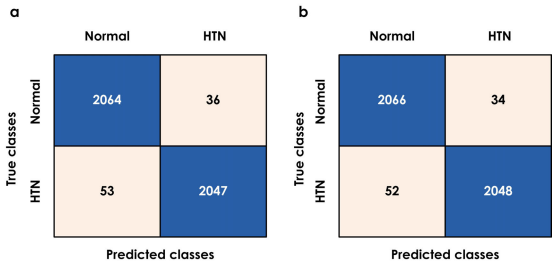

FIGURE 6. Confusion matrices using a) Bhattacharyya and b) entropy methods.

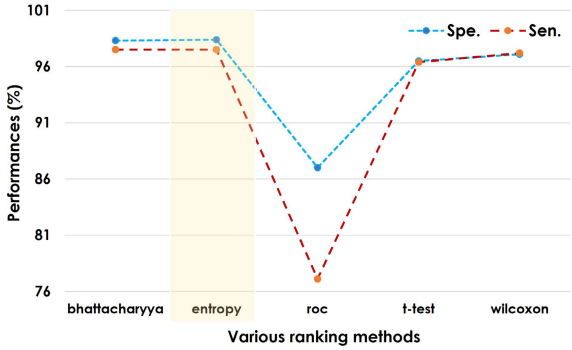

FIGURE 7. Specificity (%) and sensitivity (%) plot for various ranking approaches.

such as KNN and SVM are used to select the best possible classifier for the proposed feature model.

A. RESULTS

The problem of concern is a two-class classification problem, as it uses the feature sets for normal and HTN. Generally, there are four performance evaluation measures available for CAD systems. Hence, in this work, we have used accuracy, sensitivity, specificity, and AUC. By assessing these measures, we were able to gain a comprehensive understanding of the classification capabilities of the proposed method.

Table 2 shows the performance using KNN and SVM classifiers using different ranking approaches such as Bhattacharyya, entropy, Receiver Operating Characteristic (ROC), t-test, and Wilcoxon [52], [60], [61]. The best three classifiers from KNN and SVM classifiers are shown in Table 2. It is observed that Weighted KNN has achieved the highest accuracy of 98% using the entropy ranking method.

It is observed that the weighted KNN has achieved the highest specificity, sensitivity, and AUC of 98.4%, 97.5% and 1 respectively using the entropy method. Figure 6 shows the classification performance using confusion matrices of the best ranking methods for the weighted KNN classifier. It is observed from Figure 6 that Bhattacharya and entropy methods have the misclassification observations 89 and 86 respectively. Figure 7 shows the performances of all the ranking methods. It is observed that the accuracy of Bhattacharyya and entropy ranking methods achieved better performance as compared to other techniques.

It is also observed that the accuracy and precision of the entropy technique is 0.1% higher than the Bhattacharyya technique. Hence entropy ranking approach is considered the best ranking approach for the proposed feature extraction technique. The results exhibit that the proposed model reached promising results using shallow classifiers.

It is observed from the related work that only two works have been proposed to identify the HTN using four-chamber heart US images [30], [31]. Moreover, these works have utilized only a few US images from the patients. The sensitivity and specificity achieved by the graph embedding is 100%, however, only one image per subject is utilized [30]. A greater number of frames to cover one complete cardiac cycle is utilized and proposed GWLBP [31]. Moreover, they could be able to achieve a specificity of only 87.33%. The proposed method achieved a specificity of 98.4% by considering more number of patients. From this observation, we can conclude that the proposed system identifies almost all normal patients correctly.

V. DISCUSSION

In the present study, we have developed a handcrafted feature learning approach by combining DGMS descriptor, entropy ranking method, and shallow classifier. This provides a different dimension in the field of feature extraction technique, as it results in a classification accuracy of 98%. The proposed DGMS helps to extract significant features from the heart valve. As a result, a set of distinct features contributes to achieve remarkable system performance. Table 3 shows the mean (mn) and standard deviation (sd) of extracted features for HTN and normal classes. We have used 38% of the extracted features based on its significance ($p < 0.001$) to establish the best classification model. In Table 3 only initial 10 features are shown to restrict the area constraint for the table. Further, to show the distributions of the features scatter plot is drawn and is shown in Figure 8. It is noted that non-ranked features have achieved a classification accuracy of 78.8%. From Figure 8 it is observed that ranked DGMS features are more distinctive and more significant when compared to non-ranked features.

A. COMPARATIVE STUDY

Initially, to understand the usefulness of the Kirsch Masks (K_M), we used Frei–Chen Masks (FC_M) and Robinson Masks (R_M) [62]. Firstly, we combined(K_M) and (FC_M), and then (K_M) and (FC_M) and (R_M) are combined, it is observed that Kirsch masks alone have achieved the highest accuracy and specificity. Hence, Kirsch masks can understand the edge information in all the directions of the heart valve in a better way as compared to other masks (please refer to Table 4).

Further to show the efficiency of the proposed method we have evaluated the proposed DGMS feature descriptor against popular descriptors such as Local Binary Pattern (LBP) [63], LDP [50], and Local Optimal-Oriented Pattern (LOOP) [64]. The features obtained from these methods are ranked and classified using a weighted KNN classifier. It is observed that our proposed method has achieved 0.7%, 2.1%, and 8.2% higher results as compared to LBP, LDP, and LOOP

TABLE 2. Highest achieved accuracies (%) using different variants of KNN and SVM classifier.

Methods	KNN			SVM		
	Weighted	Cubic	Cosine	Median Gaussian	Cubic	Quadratic
Bhattacharyya	**97.9**	95.8	90.3	84	83.8	79
entropy	**98**	96	90	84.3	83.5	78.6
ROC	**82**	78	76	73	72.8	69.6
t-test	**96.5**	94.1	87.8	82.1	80.8	76.8
Wilcoxon	**97.2**	94.7	88.2	83.3	81.6	78

TABLE 3. Range (mn±sd) of DGMS features for normal and HTN with $p < 0.001$.

Features	Normal		HTN		*p-value*	Criterion
	mn	*sd*	*mn*	*sd*		
DGMS 497	47.3476	81.8940	74.9052	170.894	3.01E-11	1.3617
DGMS 753	60.0504	98.3073	79.2214	154.5059	1.66E-06	0.4641
DGMS 1009	223.5481	354.0619	350.2986	492.6916	1.71E-21	0.3235
DGMS 1265	137.394	236.1427	194.0714	301.9865	1.42E-11	0.1698
DGMS 1024	24.3714	7.8066	27.2557	8.8954	1.47E-28	0.1551
DGMS 1017	15.1285	5.8074	17.1938	6.6110	1.24E-26	0.1458
DGMS 1013	25.33	10.0260	29.0976	10.8355	4.07E-31	0.1431
DGMS 365	22.1681	6.2305	19.8195	6.1908	6.09E-34	0.1430
DGMS 1016	17.3052	6.7101	19.7357	7.3236	8.98E-29	0.1360
DGMS 1018	13.2042	5.4060	15.1966	5.7159	1.14E-30	0.1348

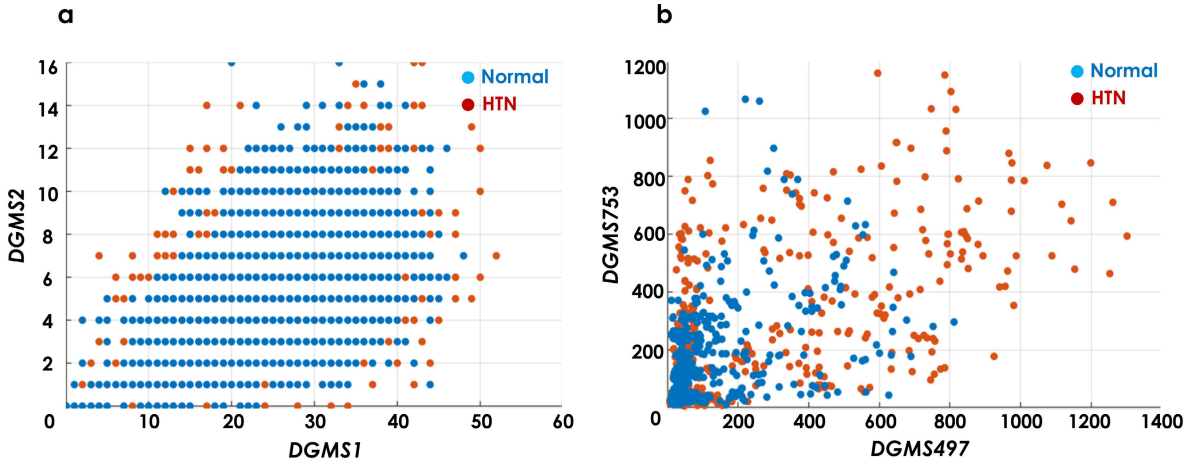

FIGURE 8. Scatter plot of a) non-ranked and b) ranked DGMS feature.

descriptors respectively. From the results, it is evident that the DGMS descriptor captures the pixel variations induced by heart valve motion effectively. The major limitations of these methods are that the pattern that is generated may repeat in the same class of images or the different locations of the same image, thereby confusing the process of classification. However, for the proposed DGMS descriptor, the binary words are generated based on the new path (as shown in Figure 5) and weights are assigned as per the combined rule based on the significance of the pixel values and mask activation. Hence the proposed approach has achieved a specificity of 98.4%.

Further, we conducted extensive experiments to evaluate the performance of various compact CNN models, including ResNet50 and ResNet50v2 [65], EfficientNetB4 [66], XceptionNet [67], DenseNet210 [68], and Inceptionv3 [69]. These models were chosen due to their proven track records of achieving exceptional results across various computer vision tasks and compactness in terms of size and parameter size [70]. To facilitate a fair comparison, we first preprocessed and fine-tuned these models on our dataset. We trained each model separately and obtained encoded vectors from the final feature extraction layers. These encoded vectors were subsequently fed into a dense classification layer. It is observed that ResNet50v2 achieved the highest accuracy of 93.8%, which is 4.2% less than the proposed approach. We have used Google Colab Pro with NVIDIA-SMI 460.32.03 Tesla T4 GPU to implement CNN models.

TABLE 4. Comparison of the proposed method with various approaches.

Methods	Acc. (%)	Spe. (%)	Sen. (%)	AUC
$K_M + FC_M$	97.8	97.4	98.3	1
$K_M + FC_M + R_M$	97.8	98.3	97.2	1
Non-ranked	78.8	75.6	82	0.88
LBP	97.3	97.5	97.1	1
LDP	95.9	96.7	95	0.99
LOOP	89.8	92	87.7	0.96
ResNet50	92.5	90.1	93	0.90
ResNet50v2	93.8	91.2	94	0.91
Inceptionv3	89.8	88.2	89.7	0.87
DenseNet201	90.6	89.2	90.8	0.89
XceptionNet	86.5	82.2	85.6	0.80
Proposed	**98**	**98.4**	**97.5**	**1**

Our evaluation process involved conducting a 10-fold cross-validation, which helped ensure the robustness of our findings. Table 4 shows the comparative analysis of various approaches. This comparative approach allowed us to draw meaningful insights into the suitability of various approaches/models for the specific classification task under investigation. It is noted that our proposed system has achieved outstanding classification accuracy when compared to other approaches. In addition, the data set is very huge, and no data augmentation technique is utilized.

Since the proposed DGMS uses the new path rule in a zig-zag way, it helps to capture pixels variation efficiently, when compared to other CNNs and feature learning methods. Thus, encourages finer coding patterns and attains an impressive performance as compared to other methods. From Table 4, we can determine that the proposed approach can be utilized in the development of AI techniques to predict the pathological condition of the heart using US images. Demonstrating subtle cardiac changes on US heart images among HTN patients may unveil the opportunity for clinicians to predict future structural or functional changes and understand the management goals and the overall prognosis. The use of a US defined model might improve diagnostic accuracy since it is independent of biological variability of the BP, technical limitations in its measurements, the effect of human errors, and may potentially eliminate the need for multiple measurements over extended periods for establishing the diagnosis.

The significant findings from the current study are listed below.

- To the best of our knowledge, this is the pioneering work in the field of automated detection of HTN using US images with huge datasets.
- We presented a substantial 2 class four-chamber heart US images, which comprises images of 2100 normal and 2100 HTN from 70 normal and 70 HTN patients, establishing the base for the HTN identification system.
- Our proposed novel DGMS feature model is suitable for the analysis of four-chamber heart US images.
- Combining the DGMS feature model with the feature ranking approach enables us to extract prominent features.
- A robust 10-fold cross-validation scheme is adopted to obtain the classification accuracy of 98% using a shallow KNN classifier.
- It does not require any GPU and thus can be deployed with minimum system requirements.

In the future, we want to perform the following with a greater number of US images.

- Producing deep features under the framework of deep neural networks with ML algorithms for the advancement of medical image analysis.
- Inherently US images pose noises, and further introducing uncertainty quantification may reduce the uncertainty while predicting various US heart images [71].
- Use of Explainable AI, to rearrange the features while performing compound classification tasks. Thus, assists the clinicians with their conclusions [72], [73].

VI. CONCLUSION

We have proposed an automated system for the detection of HTN using a handcrafted feature descriptor i.e., DGMS. This descriptor with an entropy-based ranking technique has attained remarkable accuracy and specificity of 98% and 98.4% respectively, using the KNN classifier.

Here are the key takeaways from this study:

- A new dataset of 4200 four-chamber cardiac US images from 70 healthy and 70 hypertensive patients is established, helping address the lack of database.
- A novel DGMS descriptor is proposed to capture subtle textural changes in heart walls as indicative of HTN.
- Using DGMS and feature selection, a shallow ML classifier achieved 98% accuracy in identifying HTN, outperforming deep learning models.
- The high performance suggests US imaging can discern HTN even when standard echocardiographic measures are normal or inconsistent with blood pressure.
- The automated system could aid quicker, more objective diagnosis in clinics, enabling early risk stratification and treatment through AI-assisted assessment.

In summary, this pioneering study shows an accurate automated CAD system for HTN detection is viable using cardiac US images. By addressing key data and algorithm gaps, the groundwork is laid for clinical translation and validation of these AI tools for diagnostic support. The remarkable performances paved the way for the utilization of the DGMS, encouraging the development of CAD tools using US images in the field of ML-based approaches. In addition, we plan to develop a pipeline-based handcrafted feature approach using more patients extracted from multicenter in the future.

REFERENCES

[1] Guidelines Committee, "2003 European society of hypertension–European society of cardiology guidelines for the management of arterial hypertension," *J. Hypertension*, vol. 21, no. 6, pp. 1011–1053, 2003.

[2] W. J. Elliott, "2007 guidelines for the management of arterial hypertension: The task force for the management of arterial hypertension of the European society of hypertension (ESH) and of the European society of cardiology (ESC)," *Yearbook Cardiol.*, vol. 2008, pp. 49–51, Jan. 2008.

[3] G. Mancia, R. Fagard, K. Narkiewicz, J. Redán, A. Zanchetti, M. Böhm, T. Christiaens, R. Cifkova, G. De Backer, and A. Dominiczak, "2013 Practice Guidelines for the management of arterial hypertension of the European Society of Hypertension (ESH) and the European Society of Cardiology (ESC): ESH/ESC task force for the management of arterial hypertension," *J. Hypertension*, vol. 31, no. 10, pp. 1925–1938, 2013.

[4] G. Bernotienė, V. Dulskienė, J. Klumbienė, V. Kriaučionienė, R. Kučienė, D. Lukšienė, J. Medžionienė, J. Petkevičienė, R. Radišauskas, and A. Tamošiūnas, "Worldwide trends in hypertension prevalence and progress in treatment and control from 1990 to 2019: A pooled analysis of 1201 population-representative studies with 104 million participants," *Lancet*, vol. 398, no. 10304, pp. 957–980, 2021.

[5] M. H. Forouzanfar, P. Liu, G. A. Roth, M. Ng, S. Biryukov, L. Marczak, L. Alexander, K. Estep, K. H. Abate, and T. F. Akinyemiju, "Global burden of hypertension and systolic blood pressure of at least 110 to 115 mm Hg, 1990–2015," *Jama*, vol. 317, no. 2, pp. 165–182, 2017.

[6] S. Lewington, R. Clarke, N. Qizilbash, R. Collins, and R. Peto, "Age-specific relevance of usual blood pressure to vascular mortality: A meta-analysis of individual data for one million adults in 61 prospective studies," *Lancet*, vol. 360, no. 9349, pp. 1903–1913, Dec. 2002.

[7] C. Cuspidi, E. Ambrosioni, G. Mancia, A. C. Pessina, B. Trimarco, and A. Zanchetti, "Role of echocardiography and carotid ultrasonography in stratifying risk in patients with essential hypertension: The assessment of prognostic risk observational survey," *J. Hypertension*, vol. 20, no. 7, pp. 1307–1314, 2002.

[8] R. B. Devereux and M. H. Alderman, "Role of preclinical cardiovascular disease in the evolution from risk factor exposure to development of morbid events," *Circulation*, vol. 88, no. 4, pp. 1444–1455, Oct. 1993.

[9] M. J. Roman, T. G. Pickering, J. E. Schwartz, R. Pini, and R. B. Devereux, "Association of carotid atherosclerosis and left ventricular hypertrophy," *J. Amer. College Cardiol.*, vol. 25, no. 1, pp. 83–90, Jan. 1995.

[10] C. Cuspidi, C. Valerio, C. Sala, A. Esposito, M. Masaidi, F. Negri, A. Zanchetti, and G. Mancia, "Prevalence and correlates of multiple organ damage in a never-treated hypertensive population: Role of ambulatory blood pressure," *Blood Pressure Monitor.*, vol. 13, no. 1, pp. 7–13, 2008.

[11] R. Pontremoli, M. Ravera, G. P. Bezante, F. Viazzi, C. Nicolella, V. Berruti, G. Leoncini, M. D. Sette, C. Brunelli, C. Tomolillo, and G. Deferrari, "Left ventricular geometry and function in patients with essential hypertension and microalbuminuria," *J. Hypertension*, vol. 17, no. 7, pp. 993–1000, Jul. 1999.

[12] P. Perrone-Filardi, A. Coca, M. Galderisi, S. Paolillo, F. Alpendurada, G. de Simone, E. Donal, T. Kahan, G. Mancia, J. Redon, R. Schmieder, B. Williams, and E. Agabiti-Rosei, "Noninvasive cardiovascular imaging for evaluating subclinical target organ damage in hypertensive patients: A consensus article from the European association of cardiovascular imaging, the European society of cardiology council on hypertension and the European Society of Hypertension," *J. Hypertension*, vol. 35, no. 9, pp. 1727–1741, 2017.

[13] B. Williams, "2018 ESC/ESH guidelines for the management of arterial hypertension: The task force for the management of arterial hypertension of the European society of cardiology (ESC) and the European society of hypertension (ESH)," *Eur. Heart J.*, vol. 39, no. 33, pp. 3021–3104, Sep. 2018.

[14] L. Bacharova, D. Schocken, E. Estes, and D. Strauss, "The role of ECG in the diagnosis of left ventricular hypertrophy," *Current Cardiol. Rev.*, vol. 10, no. 3, pp. 257–261, May 2014.

[15] M. Pahor, J. M. Guralnik, W. T. Ambrosius, S. Blair, D. E. Bonds, T. S. Church, M. A. Espeland, R. A. Fielding, T. M. Gill, and E. J. Groessl, "Effect of structured physical activity on prevention of major mobility disability in older adults: The life study randomized clinical trial," *Jama*, vol. 311, no. 23, pp. 2387–2396, 2014.

[16] P. M. Okin, "Regression of electrocardiographic left ventricular hypertrophy during antihypertensive treatment and the prediction of major cardiovascular events," *JAMA*, vol. 292, no. 19, p. 2343, Nov. 2004.

[17] P. M. Okin, L. Oikarinen, M. Viitasalo, L. Toivonen, S. E. Kjeldsen, M. S. Nieminen, J. M. Edelman, B. Dahlöf, and R. B. Devereux, "Prognostic value of changes in the electrocardiographic strain pattern during antihypertensive treatment: The losartan intervention for end-point reduction in hypertension study (LIFE)," *Circulation*, vol. 119, no. 14, pp. 1883–1891, Apr. 2009.

[18] G. de Simone, R. Izzo, M. Chinali, M. De Marco, G. Casalnuovo, F. Rozza, D. Girfoglio, G. L. Iovino, B. Trimarco, and N. De Luca, "Does information on systolic and diastolic function improve prediction of a cardiovascular event by left ventricular hypertrophy in arterial hypertension?" *Hypertension*, vol. 56, no. 1, pp. 99–104, Jul. 2010.

[19] M. Bombelli, R. Facchetti, C. Cuspidi, P. Villa, D. Dozio, G. Brambilla, G. Grassi, and G. Mancia, "Prognostic significance of left atrial enlargement in a general population: Results of the PAMELA study," *Hypertension*, vol. 64, no. 6, pp. 1205–1211, Dec. 2014.

[20] G. de Simone, R. Izzo, G. P. Aurigemma, M. De Marco, F. Rozza, V. Trimarco, E. Stabile, N. De Luca, and B. Trimarco, "Cardiovascular risk in relation to a new classification of hypertensive left ventricular geometric abnormalities," *J. Hypertension*, vol. 33, no. 4, pp. 745–754, 2015.

[21] T. Sehestedt, J. Jeppesen, T. W. Hansen, K. Wachtell, H. Ibsen, C. Torp-Petersen, P. Hildebrandt, and M. H. Olsen, "Risk prediction is improved by adding markers of subclinical organ damage to SCORE," *Eur. Heart J.*, vol. 31, no. 7, pp. 883–891, Apr. 2010.

[22] V. Nambi, L. Chambless, A. R. Folsom, M. He, Y. Hu, T. Mosley, K. Volcik, E. Boerwinkle, and C. M. Ballantyne, "Carotid intima-media thickness and presence or absence of plaque improves prediction of coronary heart disease risk: The ARIC (atherosclerosis risk in communities) study," *J. Amer. College Cardiol.*, vol. 55, no. 15, pp. 1600–1607, 2010.

[23] L. Van Bortel, S. Laurent, P. Boutouyrie, P. Chowienczyk, J. Cruickshank, T. De Backer, J. Filipovsky, S. Huybrechts, F. Mattace-Raso, and A. D. Protogerou, "Artery Society; European Society of Hypertension Working Group on Vascular Structure and Function; European Network for Noninvasive Investigation of Large Arteries. Expert consensus document on the measurement of aortic stiffness in daily practice using carotid-femoral pulse wave velocity," *J. Hypertens.*, vol. 30, no. 3, pp. 445–448, 2012.

[24] C. M. Clase, J. Barzilay, P. Gao, A. Smyth, R. E. Schmieder, S. Tobe, K. K. Teo, S. Yusuf, and J. F. E. Mann, "Acute change in glomerular filtration rate with inhibition of the renin-angiotensin system does not predict subsequent renal and cardiovascular outcomes," *Kidney Int.*, vol. 91, no. 3, pp. 683–690, Mar. 2017.

[25] M. Schmidt, K. E. Mansfield, K. Bhaskaran, D. Nitsch, H. T. Sørensen, L. Smeeth, and L. A. Tomlinson, "Serum creatinine elevation after renin-angiotensin system blockade and long term cardiorenal risks: Cohort study," *Brit. Med. J.*, vol. 356, p. j791, Mar. 2017.

[26] D. J. Breslin, "Prognostic importance of ophthalmoscopic findings in essential hypertension," *J. Amer. Med. Assoc.*, vol. 195, no. 5, p. 335, Jan. 1966.

[27] W. T. Longstreth, T. A. Manolio, A. Arnold, G. L. Burke, N. Bryan, C. A. Jungreis, P. L. Enright, D. O'Leary, and L. Fried, "Clinical correlates of white matter findings on cranial magnetic resonance imaging of 3301 elderly people: The cardiovascular health study," *Stroke*, vol. 27, no. 8, pp. 1274–1282, Aug. 1996.

[28] S. E. Vermeer, W. T. Longstreth, and P. J. Koudstaal, "Silent brain infarcts: A systematic review," *Lancet Neurol.*, vol. 6, no. 7, pp. 611–619, Jul. 2007.

[29] T. Unger, C. Borghi, F. Charchar, N. A. Khan, N. R. Poulter, D. Prabhakaran, A. Ramirez, M. Schlaich, G. S. Stergiou, M. Tomaszewski, R. D. Wainford, B. Williams, and A. E. Schutte, "2020 international society of hypertension global hypertension practice guidelines," *Hypertension*, vol. 75, no. 6, pp. 1334–1357, Jun. 2020.

[30] U. Raghavendra, J. K. E. Wei, A. Gudigar, A. Shetty, J. Samanth, G. Paramasivam, S. Jagadish, N. A. Kadri, M. Karabatak, Ö. Yildirim, N. Arunkumar, and A. A. Ardakani, "Automated diagnosis and assessment of cardiac structural alteration in hypertension ultrasound images," *Contrast Media Mol. Imag.*, vol. 2022, pp. 1–10, May 2022.

[31] A. Gudigar, U. Raghavendra, T. Devasia, K. Nayak, S. M. Danish, G. Kamath, J. Samanth, U. M. Pai, V. Nayak, R. S. Tan, E. J. Ciaccio, and U. R. Acharya, "Global weighted LBP based entropy features for the assessment of pulmonary hypertension," *Pattern Recognit. Lett.*, vol. 125, pp. 35–41, Jul. 2019.

[32] U. Raghavendra, H. Fujita, A. Gudigar, R. Shetty, K. Nayak, U. Pai, J. Samanth, and U. R. Acharya, "Automated technique for coronary artery disease characterization and classification using DD-DTDWT in ultrasound images," *Biomed. Signal Process. Control*, vol. 40, pp. 324–334, Feb. 2018.

[33] U. Raghavendra, U. R. Acharya, A. Gudigar, R. Shetty, N. Krishnananda, U. Pai, J. Samanth, and C. Nayak, "Automated screening of congestive heart failure using variational mode decomposition and texture features extracted from ultrasound images," *Neural Comput. Appl.*, vol. 28, no. 10, pp. 2869–2878, Oct. 2017.

[34] A. Gudigar, J. Samanth, A. Vasudeva, K. Nayak, R.-S. Tan, E. J. Ciaccio, C. P. Ooi, P. D. Barua, F. Molinari, and U. R. Acharya, "Role of four-chamber heart ultrasound images in automatic assessment of fetal heart: A systematic understanding," *Informatics*, vol. 9, no. 2, p. 34, Apr. 2022.

[35] F. López-Martínez, E. R. Núñez-Valdez, R. G. Crespo, and V. García-Díaz, "An artificial neural network approach for predicting hypertension using NHANES data," *Sci. Rep.*, vol. 10, no. 1, Jun. 2020, Art. no. 10620.

[36] K. Dashdondov and M.-H. Kim, "Mahalanobis distance based multivariate outlier detection to improve performance of hypertension prediction," *Neural Process. Lett.*, vol. 55, no. 1, pp. 265–277, Feb. 2023.

[37] G. Paragliola and A. Coronato, "An hybrid ECG-based deep network for the early identification of high-risk to major cardiovascular events for hypertension patients," *J. Biomed. Informat.*, vol. 113, Jan. 2021, Art. no. 103648.

[38] H. Tang, Y. Jiang, T. Li, and X. Wang, "Identification of pulmonary hypertension using entropy measure analysis of heart sound signal," *Entropy*, vol. 20, no. 5, p. 389, May 2018.

[39] C. Chen, H. Y. Zhao, S. H. Zheng, R. A. Ramachandra, X. He, Y. H. Zhang, and V. K. Sudarshan, "Interpretable hybrid model for an automated patient-wise categorization of hypertensive and normotensive electrocardiogram signals," *Comput. Methods Programs Biomed. Update*, vol. 3, Apr. 2023, Art. no. 100097.

[40] Y. Chu, K. Tang, Y.-C. Hsu, T. Huang, D. Wang, W. Li, S. I. Savitz, X. Jiang, and S. Shams, "Non-invasive arterial blood pressure measurement and SpO_2 estimation using PPG signal: A deep learning framework," *BMC Med. Informat. Decis. Making*, vol. 23, no. 1, p. 131, Jul. 2023.

[41] M. Zhang, T. Zhang, and Y. Cheng, "Intelligent method of non-invasive detection and grading of hypertension using fingertip photoplethysmography," in *Proc. 3rd Int. Conf. Appl. Mach. Learn. (ICAML)*, Jul. 2021, pp. 418–422.

[42] E. Kogan, E.-M. Didden, E. Lee, A. Nnewihe, D. Stamatiadis, S. Mataraso, D. Quinn, D. Rosenberg, C. Chehoud, and C. Bridges, "A machine learning approach to identifying patients with pulmonary hypertension using real-world electronic health records," *Int. J. Cardiol.*, vol. 374, pp. 95–99, Mar. 2023.

[43] K. Gupta, V. Bajaj, and I. A. Ansari, "A support system for automatic classification of hypertension using BCG signals," *Expert Syst. Appl.*, vol. 214, Mar. 2023, Art. no. 119058.

[44] E. Martinez-Ríos, L. Montesinos, M. Alfaro-Ponce, and L. Pecchia, "A review of machine learning in hypertension detection and blood pressure estimation based on clinical and physiological data," *Biomed. Signal Process. Control*, vol. 68, Jul. 2021, Art. no. 102813.

[45] A. Leha, K. Hellenkamp, B. Unsöld, S. Mushemi-Blake, A. M. Shah, G. Hasenfuß, and T. Seidler, "A machine learning approach for the prediction of pulmonary hypertension," *PLoS ONE*, vol. 14, no. 10, Oct. 2019, Art. no. e0224453.

[46] X.-L. Zou, Y. Ren, D.-Y. Feng, X.-Q. He, Y.-F. Guo, H.-L. Yang, X. Li, J. Fang, Q. Li, J.-J. Ye, L.-Q. Han, and T.-T. Zhang, "A promising approach for screening pulmonary hypertension based on frontal chest radiographs using deep learning: A retrospective study," *PLoS ONE*, vol. 15, no. 7, Jul. 2020, Art. no. e0236378.

[47] M. Recenti, C. Ricciardi, K. J. Edmunds, M. K. Gislason, S. Sigurdsson, U. Carraro, and P. Gargiulo, "Healthy aging within an image: Using muscle radiodensitometry and lifestyle factors to predict diabetes and hypertension," *IEEE J. Biomed. Health Informat.*, vol. 25, no. 6, pp. 2103–2112, Jun. 2021.

[48] A. Gudigar, R. U, J. Samanth, M. R. Gangavarapu, A. Kudva, G. Paramasivam, K. Nayak, R.-S. Tan, F. Molinari, E. J. Ciaccio, and U. R. Acharya, "Automated detection of chronic kidney disease using image fusion and graph embedding techniques with ultrasound images," *Biomed. Signal Process. Control*, vol. 68, Jul. 2021, Art. no. 102733.

[49] A. Gudigar, J. Samanth, U. Raghavendra, C. Dharmik, A. Vasudeva, R. Padmakumar, R.-S. Tan, E. J. Ciaccio, F. Molinari, and U. R. Acharya, "Local preserving class separation framework to identify gestational diabetes mellitus mother using ultrasound fetal cardiac image," *IEEE Access*, vol. 8, pp. 229043–229051, 2020.

[50] T. Jabid, M. H. Kabir, and O. Chae, "Gender classification using local directional pattern (LDP)," in *Proc. 20th Int. Conf. Pattern Recognit.*, Aug. 2010, pp. 2162–2165.

[51] C. Sammut and G. I. Webb, *Encyclopedia of Machine Learning*. Cham, Switzerland: Springer, 2011.

[52] S. Theodoridis, "Konstantinos koutroumbas," in *Pattern Recognition*. Amsterdam, The Netherlands: Elsevier, 2003.

[53] L. E. Peterson, "K-nearest neighbor," *Scholarpedia*, vol. 4, no. 2, p. 1883, 2009.

[54] W. S. Noble, "What is a support vector machine," *Nature Biotechnol.*, vol. 24, no. 12, pp. 1565–1567, Dec. 2006.

[55] J. M. Johnson and A. Yadav, "Fault detection and classification technique for HVDC transmission lines using KNN," in *Information and Communication Technology for Sustainable Development: Proceedings of ICT4SD 2016*, vol. 2. Cham, Switzerland: Springer, 2018, pp. 245–253.

[56] (2015). *Statistics and Machine Learning Toolbox for MATLAB; Mathworks: Natick, MA, USA*. Accessed: Oct. 13, 2023. [Online]. Available: https://es.mathworks.com/help/pdf_doc/stats/stats.pdf

[57] B. Scholkopf, K.-K. Sung, C. J. C. Burges, F. Girosi, P. Niyogi, T. Poggio, and V. Vapnik, "Comparing support vector machines with Gaussian kernels to radial basis function classifiers," *IEEE Trans. Signal Process.*, vol. 45, no. 11, pp. 2758–2765, Nov. 1997.

[58] S.-L. Lin, "Application of machine learning to a medium Gaussian support vector machine in the diagnosis of motor bearing faults," *Electronics*, vol. 10, no. 18, p. 2266, Sep. 2021.

[59] D.-X. Zhou and K. Jetter, "Approximation with polynomial kernels and SVM classifiers," *Adv. Comput. Math.*, vol. 25, nos. 1–3, pp. 323–344, Jul. 2006.

[60] H. Liu and H. Motoda, *Feature Selection for Knowledge Discovery and Data Mining*, vol. 454. Cham, Switzerland: Springer, 2012.

[61] D. T. Ross, U. Scherf, M. B. Eisen, C. M. Perou, C. Rees, P. Spellman, V. Iyer, S. S. Jeffrey, M. Van de Rijn, M. Waltham, A. Pergamenschikov, J. C. F. Lee, D. Lashkari, D. Shalon, T. G. Myers, J. N. Weinstein, D. Botstein, and P. O. Brown, "Systematic variation in gene expression patterns in human cancer cell lines," *Nature Genet.*, vol. 24, no. 3, pp. 227–235, Mar. 2000.

[62] I. El Khadiri, Y. El Merabet, Y. Ruichek, D. Chetverikov, R. El Mokhtar, and A. S. Tarawneh, "Local ternary pattern based multi-directional guided mixed mask (MDGMM-LTP) for texture and material classification," *Expert Syst. Appl.*, vol. 205, Nov. 2022, Art. no. 117646.

[63] T. Ojala, M. Pietikainen, and D. Harwood, "Performance evaluation of texture measures with classification based on Kullback discrimination of distributions," in *Proc. 12th Int. Conf. Pattern Recognit.*, Oct. 1994, pp. 582–585.

[64] T. Chakraborti, B. McCane, S. Mills, and U. Pal, "LOOP descriptor: Local optimal-oriented pattern," *IEEE Signal Process. Lett.*, vol. 25, no. 5, pp. 635–639, May 2018.

[65] K. He, X. Zhang, S. Ren, and J. Sun, "Deep residual learning for image recognition," in *Proc. IEEE Conf. Comput. Vis. Pattern Recognit. (CVPR)*, Jun. 2016, pp. 770–778.

[66] M. Tan and Q. Le, "EfficientNet: Rethinking model scaling for convolutional neural networks," in *Proc. Int. Conf. Mach. Learn.*, 2019, pp. 6105–6114.

[67] F. Chollet, "Xception: Deep learning with depthwise separable convolutions," in *Proc. IEEE Conf. Comput. Vis. Pattern Recognit. (CVPR)*, Jul. 2017, pp. 1800–1807.

[68] G. Huang, Z. Liu, L. Van Der Maaten, and K. Q. Weinberger, "Densely connected convolutional networks," in *Proc. IEEE Conf. Comput. Vis. Pattern Recognit. (CVPR)*, Jul. 2017, pp. 2261–2269.

[69] C. Szegedy, V. Vanhoucke, S. Ioffe, J. Shlens, and Z. Wojna, "Rethinking the inception architecture for computer vision," in *Proc. IEEE Conf. Comput. Vis. Pattern Recognit. (CVPR)*, Jun. 2016, pp. 2818–2826.

[70] *Keras Documentation: Keras Applications Keras.IO*. Accessed: Oct. 2, 2023. [Online]. Available: https://keras.io/api/applications/

[71] M. Abdar, F. Pourpanah, S. Hussain, D. Rezazadegan, L. Liu, M. Ghavamzadeh, P. Fieguth, X. Cao, A. Khosravi, U. R. Acharya, V. Makarenkov, and S. Nahavandi, "A review of uncertainty quantification in deep learning: Techniques, applications and challenges," *Inf. Fusion*, vol. 76, pp. 243–297, Dec. 2021.
[72] R. Rodríguez-Pérez and J. Bajorath, "Interpretation of machine learning models using Shapley values: Application to compound potency and multi-target activity predictions," *J. Comput.-Aided Mol. Des.*, vol. 34, no. 10, pp. 1013–1026, Oct. 2020.
[73] H. W. Loh, C. P. Ooi, S. Seoni, P. D. Barua, F. Molinari, and U. R. Acharya, "Application of explainable artificial intelligence for healthcare: A systematic review of the last decade (2011–2022)," *Comput. Methods Programs Biomed.*, vol. 226, Nov. 2022, Art. no. 107161.

ANJAN GUDIGAR received the Ph.D. degree from the Manipal Academy of Higher Education, India. He is currently a Faculty Member with the Department of Instrumentation and Control Engineering, Manipal Institute of Technology, Manipal, India. He has published several research papers in international conferences and journals. His research interests include image processing, medical image analysis, and pattern recognition. For more details please visit http://scholar.google.co.in/citations?user=qoe6EvsAAAAJ&hl=en.

NAHRIZUL ADIB KADRI received the B.B.Eng. degree from the University of Malaya, Malaysia, in 2001, the M.Biomed.E. degree from The University of New South Wales, Australia, in 2003, and the Ph.D. degree in microengineering from the University of Surrey, U.K., in 2011. His current research interests include BioMEMS and lab-on-chip, particularly in the development of low-cost and practical devices for characterization of cell populations and diagnostic applications. He is also interested in the use of computers in biomedical engineering and healthcare in general; particularly in the areas of web technology, health information systems, and microprocessors. His ISI-indexed publications may be viewed at http://www.researcherid.com/rid/D-4400-2009.

U. RAGHAVENDRA received the Ph.D. degree from the Manipal Academy of Higher Education, India. He is a Faculty Member with the Department of Instrumentation and Control Engineering, Manipal Institute of Technology, Manipal, India. He has published several papers in refereed international SCI-IF journals and international conference proceedings. He has a patent to his credit. His major academic interests are in 3-D computer vision, image processing, and medical image analysis. He received the Invention Award from Intellectual Ventures, USA, for his innovations, in 2014. For more details please visit https://scholar.google.co.in/citations?user=3nzcDREAAAAJ&hl=en.

JYOTHI SAMANTH received the Ph.D. degree from the Manipal Academy of Higher Education, India. She is a Faculty Member with the Department of Cardiovascular Technology, Manipal College of Health Professions, Manipal Academy of Higher Education. She has several publications to her credit, especially in the field of cardiology and echocardiography. Her research interest includes advances in fetal and adult echocardiographic techniques. For more details please visit https://scholar.google.com/citations?hl=en&user=Knbk8q4AAAAJ.

MAHESH ANIL INAMDAR is currently pursuing the Ph.D. degree in the prospects of artificial intelligence in health care (ischemic brain strokes). He is also a Faculty Member with the Department of Mechatronics. He has industrial experience as a data scientist in machine learning work domain. His research interest includes development of intelligence systems, which can improve and revolutionize the current healthcare systems. For more details please visit https://scholar.google.com/citations?user=Aru-8wQAAAAJ&hl=en.

MUKUND A. PRABHU received the D.M. degree in cardiology and the P.D.F. degree in cardiac electrophysiology from the Sree Chitra Thirunal Institute for Medical Science, India. He has completed a clinical fellowship in cardiac electrophysiology and pacing from the Royal Melbourne Hospital, Australia. He is an Associate Professor and a Consultant Electrophysiologist with the Department of Cardiology, Kasturba Medical College, Manipal Academy of Higher Education, Manipal, India. His focus on research includes cardiac electrophysiology, cardiac arrhythmias, cardiac pacing, and defibrillators. For more details please visit https://pubmed.ncbi.nlm.nih.gov/?term=prabhu+m+a.

U. RAJENDRA ACHARYA received the Ph.D., D.Eng., and D.Sc. degrees. He is a Professor (artificial intelligence in healthcare) with the University of Southern Queensland, Australia; a Distinguished Professor with the International Research Organization for Advanced Science and Technology, Kumamoto University, Japan; and an Adjunct Professor with the University of Malaya, Malaysia, and Asia University, Taiwan. His funded research has accrued cumulative grants exceeding six million Singapore dollars. He has authored over 600 publications, including 550 in refereed international journals, 42 in international conference proceedings, and 17 books. He has received more than 70,000 citations on Google Scholar (with an H-index of 132). He has ranked in the top 1% of the highly cited researchers for the last seven consecutive years (2016–2022) in computer science, according to the Essential Science Indicators of Thomson. His research interests include biomedical imaging and signal processing, data mining, visualization, and the applications of biophysics for better healthcare design and delivery. He is on the editorial boards of many journals and has served as a guest editor for several AI-related issues.